OPEN ACCESS

Geophysics & Space ARTICLE

The Innovation Geoscience

Auroral activity observed from unusual latitudes in China and its underlying significance

Jiaojiao Zhang,[1,2,3,*] Xiang Deng,[1,2,3] Jiyao Xu,[1,2] Hui Li,[1,2] Hang Li,[1,2,3] Wei Wang,[1,3] Jianyun Liang,[1,2] Simon G. Shepherd,[4] Evan G. Thomas,[4] Ailan Lan,[1,2,3] Jingye Yan,[1,2] Zheng Wang,[1,2,3] Qing-He Zhang,[1,2] Ziqian Liu,[1] Xinyue Wang,[5] Fuqing Huang,[6] Xianguo Zhang,[5] Weiguo Zong,[7] and Chi Wang[1,2,*]

*Correspondence: jjzhang@spaceweather.ac.cn (J.Z.); cw@spaceweather.ac.cn (C.W.)

Received: June 24, 2025; Accepted: January 14, 2026; Published Online: January 15, 2026; https://doi.org/10.59717/j.xinn-geo.2026.100197

GRAPHICAL ABSTRACT

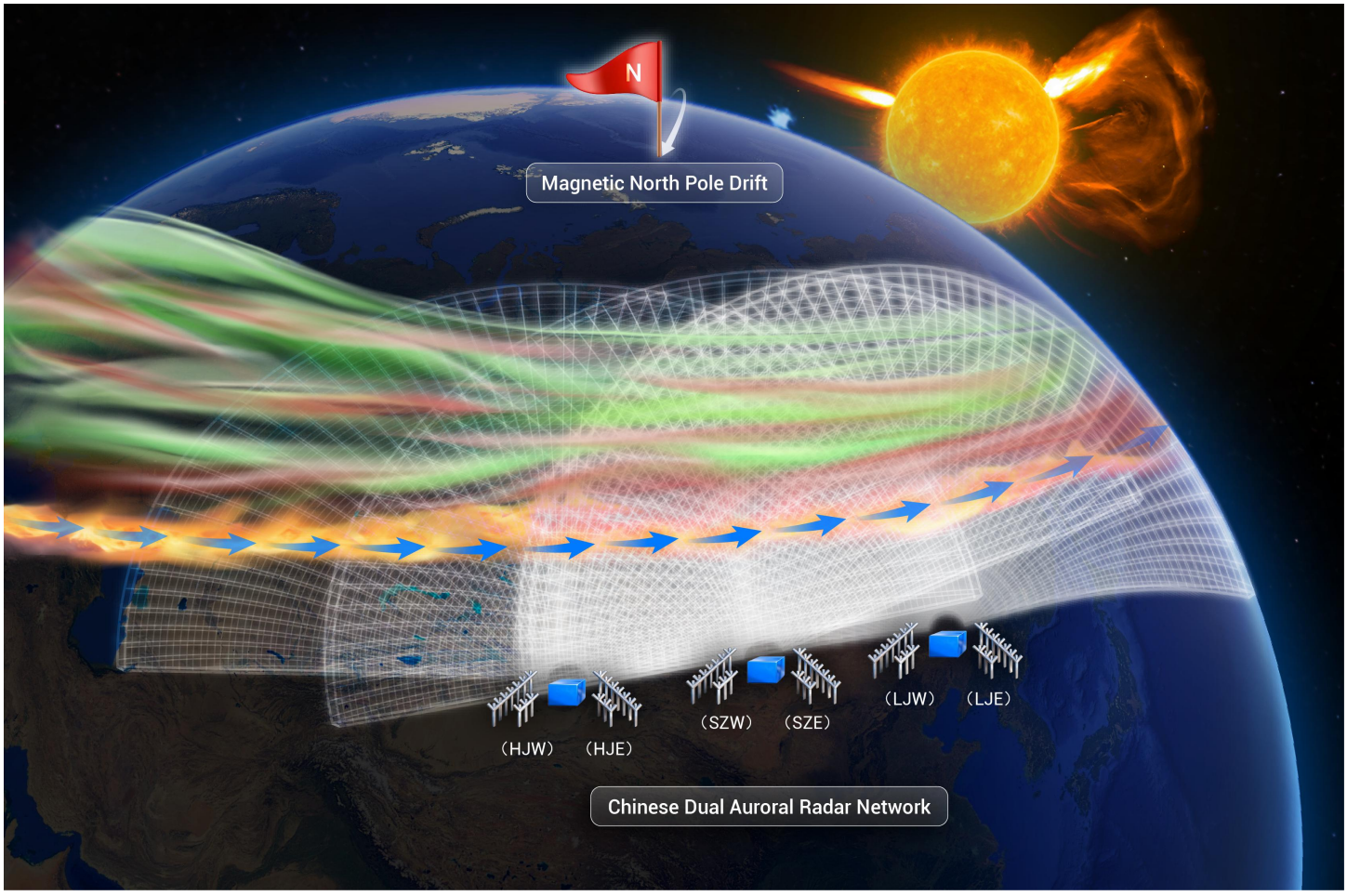

PUBLIC SUMMARY

- Spectacular auroras were spotted at unusual latitudes in China during a severe geomagnetic storm.
- CN-DARN reveals the link of auroral intensification to dawnside subauroral polarization (SAPS) streams.
- CN-DARN observed high-speed ionospheric irregularities driven by dawnside SAPS invading China's airspace.

ARTICLE Geophysics & Space

OPEN ACCESS

www.the-innovation.org/geoscience

Auroral activity observed from unusual latitudes in China and its underlying significance

Jiaojiao Zhang,[1,2,3,*] Xiang Deng,[1,2,3] Jiyao Xu,[1,2] Hui Li,[1,2] Hang Li,[1,2,3] Wei Wang,[1,3] Jianyun Liang,[1,2] Simon G. Shepherd,[4] Evan G. Thomas,[4] Ailan Lan,[1,2,3] Jingye Yan,[1,2] Zheng Wang,[1,2,3] Qing-He Zhang,[1,2] Ziqian Liu,[1] Xinyue Wang,[5] Fuqing Huang,[6] Xianguo Zhang,[5] Weiguo Zong,[7] and Chi Wang[1,2,*]

[1]State Key Laboratory of Solar Activity and Space Weather, National Space Science Center, Chinese Academy of Sciences, Beijing 100190, China

[2]University of Chinese Academy of Sciences, Beijing 101408, China

[3]Siziwang Observatory of Space Weather, National Space Science Center, Chinese Academy of Sciences, Ulanqab 011828, China

[4]Thayer School of Engineering, Dartmouth College, Hanover, New Hampshire 03755, USA

[5]Beijing Key Laboratory of Space Environment Exploration, National Space Science Center, Chinese Academy of Sciences, Beijing 100190, China

[6]Deep Space Exploration Laboratory/School of Earth and Space Sciences, University of Science and Technology of China, Hefei 230026, China

[7]Key Laboratory of Space Weather, National Satellite Meteorological Center (National Center for Space Weather), China Meteorological Administration, Beijing 100081, China

*Correspondence: jjzhang@spaceweather.ac.cn (J.Z.); cw@spaceweather.ac.cn (C.W.)

Received: June 24, 2025; Accepted: January 14, 2026; Published Online: January 15, 2026; https://doi.org/10.59717/j.xinn-geo.2026.100197

Citation: Zhang J., Deng X., Xu J., et al. (2026). Auroral activity observed from unusual latitudes in China and its underlying significance. *The Innovation Geoscience* **4**:100197.

Auroras have been observed at unusual latitudes of China over the past couple of years, which may be a direct result of the north magnetic pole's drift and intense solar activity. However, the specific impact on the Asian space environment remains unknown. Here, we present auroral activities recorded in southern Inner Mongolia (~37.2° N in magnetic latitude) and the resulting ionospheric environmental changes detected by the Chinese Dual Auroral Radar Network (CN-DARN) during a recent severe geomagnetic storm. Leveraging the wide spatial coverage and continuous high time resolution monitoring capabilities of the CN-DARN, comprehensive analysis of ground-based and space-based multi-source data reveals that CN-DARN has captured the spatiotemporal evolution characteristics of dawn-side subauroral polarization streams (SAPS). The study identifies a direct link between auroral intensification and dawnside SAPS acceleration for the first time, establishing a mechanistic connection between auroral activity and ionospheric convection dynamics in subauroral region. Moreover, the observations show that the ionospheric irregularities with high velocity of 1,000 m/s induced by the dawnside SAPS have propagated to Mohe (~ 48.6° N in magnetic latitude), the northernmost region of China. The research also reveals that intense auroral particle precipitation caused severe degradation of high-frequency (HF) communications in the Asian region. This study represents the first comprehensive investigation of auroral activity observed at unusual latitudes of China, unraveling the impact of auroral activities on the ionospheric environment of Asian mid-to-high latitudes. It also showcases the critical capabilities of the Chinese Meridian Project in addressing space environmental challenges of Asia.

INTRODUCTION

Solar eruptions cause geomagnetic storms, creating splendid auroras in the polar regions of the Earth. The magnetic field lines of the Earth converge in the polar regions and extend nearly perpendicular towards space. Therefore, the high-energy particles in the solar wind and in the Earth's magnetosphere can directly enter the Earth's northern and southern polar regions and collide with the molecules or atoms in the atmosphere, creating the colorful light displays we see as aurora. Earth's aurora occurs around the magnetic pole in oval-shaped belts, and is usually confined to the high-latitude regions of 60~70 degrees.[1] However, when a strong solar storm hits the Earth, the auroral oval will expand rapidly into lower latitude regions, causing dramatic changes in the ionospheric environment and producing disturbances and large numbers of ionospheric irregularities. The electron density irregularities in the ionosphere with scale sizes ranging from hundreds of kilometers to meters can disrupt radio communications, over-the-horizon radar detection, and global navigation satellite systems that rely on or pass through the ionosphere to transmit electromagnetic waves.

The historical north magnetic pole was located in the Canadian Arctic region, resulting in the geomagnetic latitude in most of Asia being lower than the geographic latitude. During periods of high solar activity, aurora were only visible in high latitude region of northern China, such as Mohe (~53° N in geographic latitude (GLAT)) in Heilongjiang Province. Similarly, in Japan, they could only be witnessed in Hokkaido, the northernmost island. Recently, aurora have been observed in areas of Asia that are not usually known for seeing aurora, such as the southern region of Inner Mongolia (GLAT:40°~41° N) and Beijing (GLAT: 39°~41° N) of China, Tohoku (GLAT: 38°~42° N) and Chubu (GLAT: 35°~38° N) of Japan.[2] This is partly due to the ascending phase of the 25th Solar Cycle, during which solar activity has become much more intense. This may also partly due to the fast shift of the north magnetic pole from Northern Canada toward Eastern Siberia, which is attributed to fast fluid flows in the Earth's outer core, especially in the North polar region.[3] The north magnetic pole, the location where the magnetic field points vertically downwards, was located in the Canadian Arctic when the first in situ measurements were made in 1831.[4] The pole has moved toward Siberia at a speed of 0-15 km per year historically.[5] However, its movement speed has accelerated to 50-60 km per year since 1990, crossing the international date line in October 2017 and is continuing to move southward. The accelerated drift of the north magnetic pole resulted in the out-of-Cycle update in 2019 of the World Magnetic Model used for navigation in many mobile devices.[6] By integrating an empirical data-driven magnetospheric magnetic field model with a suite of internal International Geomagnetic Reference Field (IGRF) models, the secular evolution of the northern and southern auroral ovals over the 1965–2020 time period has been investigated. The study found that the Northern auroral oval shifted approximately of 4 degrees in the plane of the ~100° geographic meridian over the 55-year period, due to the drift of the north magnetic pole.[7] This implies that as the auroral ovals undergo a secular shift toward lower latitudes in Asia, auroras will be more easily visible in the mid-latitude regions of Asia. The geomagnetic latitude of Asia has become increasingly higher than before. However, specific influences of the drift of the Earth's north magnetic pole on the space environment in the Asian region have not been reported to date.

Caused by a coronal mass ejection (CME), a strong geomagnetic storm occurred on October 10-11, 2024, sending brilliant auroral displays into the night skies at unusual latitudes of northern China, such as Inner Mongolia and Beijing—its visibility extending far beyond the usual regions. Scientist at the Siziwang Observatory of Space Weather (GLAT~41.8°N) in Inner Mongolia Autonomous Region recorded continuously the spectacular auroral activities by using cameras. Meanwhile, an all-sky imager of the Chinese Meridian Project (CMP) deployed at the Observatory also recorded the auroral activities. Simultaneously with the optical auroral measurements, numerous ionospheric irregularities emerged within the fields of view (FOVs) of the newly built Chinese Dual Auroral Radar Network (CN-DARN) of the CMP and rapidly drifted with auroral activities. The CN-DARN consists of three pairs of high-frequency coherent scatter radars deployed at Longjing (Jilin Province), Siziwang (Inner Mongolia Autonomous Region), and Hejing (Xinjiang Uygur Autonomous Region), providing continuous monitoring of ionospheric disturbances and the drift of ionospheric irregularities over the middle to high latitudes of the Asian region.[8] Extending longitudinally over ~9 hours of local time and spanning the middle-to-high latitudes of Asia above 40° magnetic latitude (MLAT), the CN-DARN conceived as one of key parts of the CMP Phase II.[9] On one hand, it acts as a bridge linking the polar regions and the

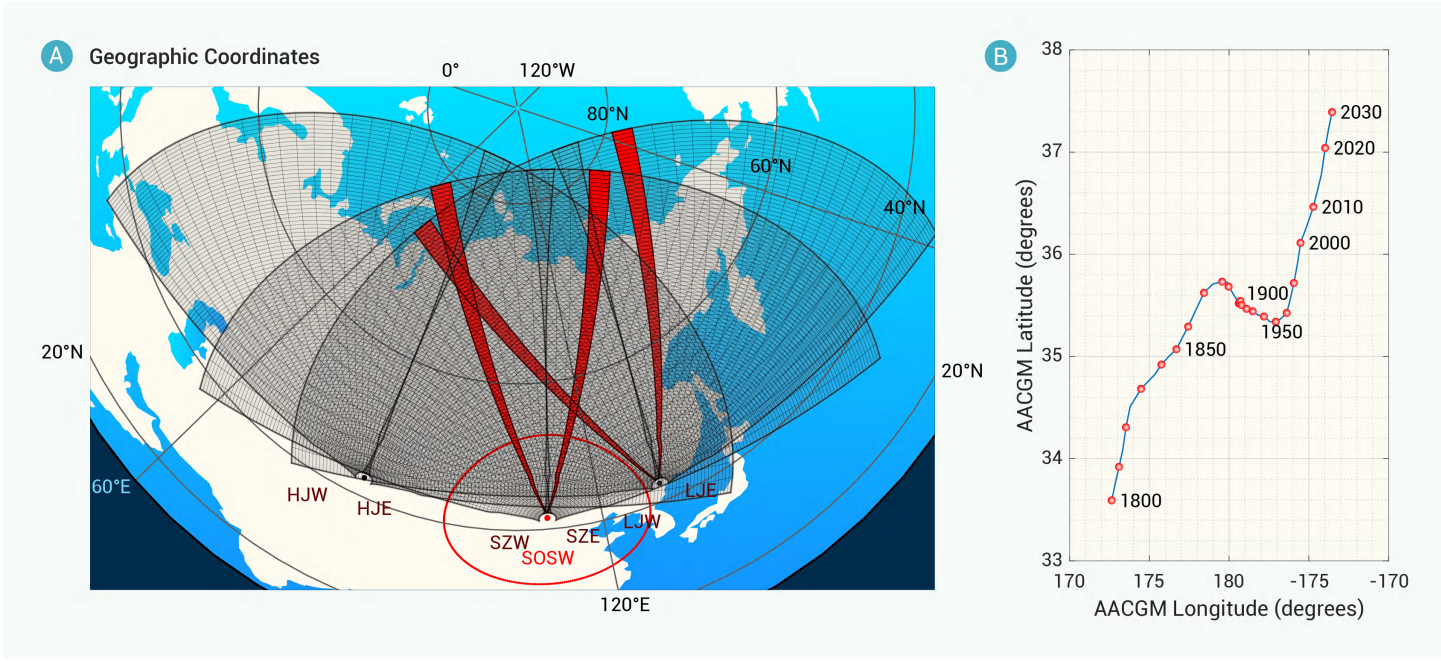

Figure 1. The fields-of-view (FOVs) of the six CN-DARN radars and the variation of the geomagnetic coordinates for the Siziwang Observatory of Space Weather (SOSW) (A) Beam 3 of the Longjing East radar (LJE), beam 15 of the Longjing West radar (LJW), beam 3 of the Siziwang East radar (SZE), and beam 18 of the Siziwang West radar (SZW) are highlighted in red. The red circle indicates the FOV of the 630 nm all-sky airglow imager deployed at SOSW. (B) The path of the AACGM coordinates for the SOSW from the year 1800 to 2030.

space monitoring network in middle and low latitudes of China, enabling the CMP to monitor the propagation and coupling effects of ionospheric disturbances across high, middle and low latitudes. On the other hand, the establishment of the CN-DARN filled the long-lasting extensive detection gap of the Super Dual Auroral Radar Network (SuperDARN)[10,11] in Asia, enabling us to obtain a complete global-scale image of the dynamic drift of ionospheric irregularities. The preliminary observation results of the CN-DARN have demonstrated its ability in monitoring and studying ionospheric irregularities, subauroral polarization streams (SAPS), traveling ionospheric disturbances (TIDs) and large-scale ionospheric convection.[8]

In this paper, the auroral activity recorded from unusual latitude of China and the resulting ionospheric environment disturbances detected by the CN-DARN of the CMP during the severe geomagnetic storm on 10 October 2024 are reported for the first time. We further integrated multi-source data from the ground-based auroral optical detection, satellite-based auroral imaging and particle precipitation detection, and CN-DARN's ionospheric dyniamic monitoring to analyze the correlation between auroral activities and fast ionospheric irregularity drifts, and deeply explore the impact of auroral activities on high-frequency (HF) communications in the Asian region.

MATERIALS AND METHODS

The auroral images were recorded by a SONY ILCE-7C camera with exposure time of 15s at the Siziwang Observatory of Space Weather (41.8°N, 111.9°E in geographic coordinates) on 10 October 2024. The image data is: ISO-4000, focal length: 24 mm, aperture: f/4, exposure time:15 s. An airglow all-sky imager at the observatory, which consists of a filter (630.0 nm) on a wheel, a fish-eye lens with a field of view of 180° and Charge Coupled Device (CCD) detector with 1,024 × 1,024 pixel, also recorded the aurora activity on that day. The integration time of the imager is 2 min.

The three pairs of CN-DARN radars are located at three observatories: Longjing (42.8° N, 129.4°E in geographic coordinates), Jilin Province; Siziwang (41.8° N, 111.9° E), Inner Mongolia Autonomous Region; and Hejing (42.8° N, 83.7° E), Xinjiang Uygur Autonomous Region. The radar transmitting and receiving array (main antenna array) consists of 16 broadband (8-20 MHz) twin-terminated folded dipole (TTFD) antennas with a corner reflector, while the interferometry array of four TTFD antennas located behind the main array only receive backscattered signals. The radars receive signals backscattered by decameter-scale ionospheric irregularities and the line-of-sight (LOS) Doppler velocity of the irregularities can be measured from the frequency shift in the returned signals.[12] In common mode, the beam formed by the main array is directed into 24 directions with angular separation between beams of 3.25°. The maximum range is set to 100 range gates, with the range resolution of 45 km. The FOV of one radar extends 78° in angular direction and from 180 km to 4500 km in range. The temporal resolution is defined by the azimuth scan and is typically 1 min. The FOVs of the six CN-DARN radars and the 630 nm airglow all-sky imager in geographic coordinates are shown in Figure 1A. Beam 3 of the Siziwang East (SZE) radar, beam 18 of the Siziwang West (SZW) radar, beam 3 of the Longjing East (LJE) radar, and beam 15 of the Longjing West (LJW) radar are highlighted in red. During the period shown, there was a power outage in Hejing County, and no observations were made by the Hejing East (HJE) and Hejing West (HJW) radars.

The path of the altitude-adjusted corrected geomagnetic (AACGM) coordinates[13] for the Siziwang Observatory of Space Weather from the year of 1800 to 2030 is shown in Figure 1B. The magnetic latitude of the observatory has undergone a remarkable northward shift and is persistently moving towards higher latitudes. The latest 14th generation of International Geomagnetic Reference Field (IGRF) model were used in the AACGM coordinates calculation. The 14th generation of IGRF model contains coefficients from 1900-2025, with extrapolation used to 2030. For the period before 1900, the coefficients derived from the magnetic field model described by Jonkers et al.[14] are used in the AACGM coordinates calculation. The geomagnetic latitude of the Siziwang Observatory of Space Weather is becoming increasingly higher, which is also the case in most regions of Asia.

The auroral images taken by the Special Sensor Ultraviolet Spectrographic Image (SSUSI) on board the Defense Meteorological Satellite Program (DMSP) satellite Flight 17 and Flight 18 are used to compare the locations of the auroral oval and the ionospheric irregularities detected by the CN-DARN radars. The SSUSI instrument is a hyperspectral cross-track scanning spectrometer that measures auroral emission at five far-ultraviolet spectral bins: N2 Lyman–Birge–Hopfield short-band (LBHS, 140–152 nm), Lyman–Birge–Hopfield long-band (LBHL, 164–180 nm), O (130.4 nm), O (135.6 nm), and H (121.6 nm).[15] Aurora images taken by SSUSI in the LBHS band are used in this study.

The fluxes and energy spectral distributions of precipitating particles observed by plasma analyzer (PMA) onboard the Fengyun-3E (FY-3E) mete-

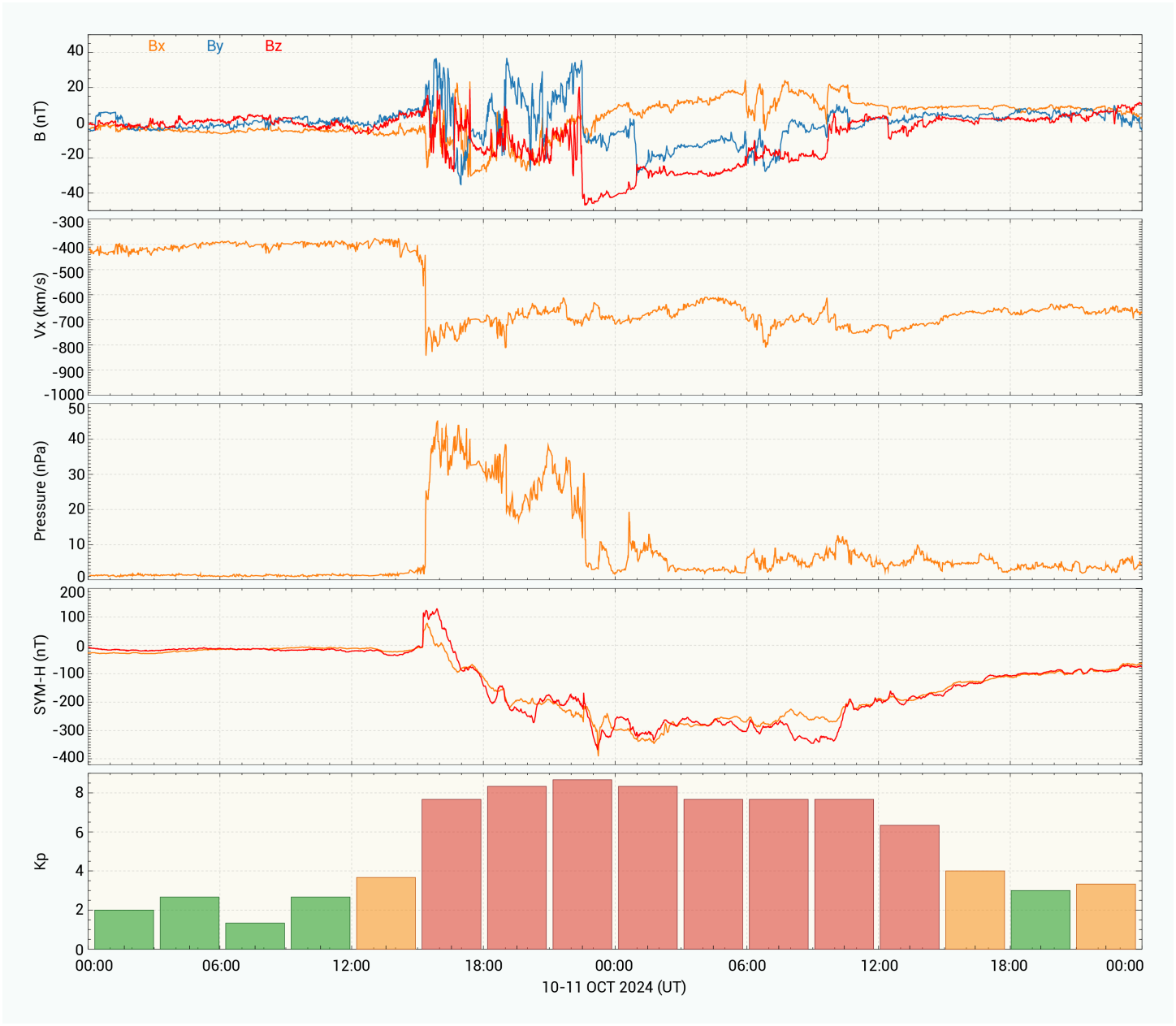

Figure 2. Solar wind conditions and geomagnetic indices during 10-11 October 2024 From top to bottom, they are the three components of IMF, solar wind velocity, solar wind dynamic pressure at the bow shock nose, SYM-H and Kp index. The red curve in the SYM-H panel is a similar SYM-H index calculated from magnetometers of the Chinese Meridian Project.

orological satellite are used in this study. The data of the special sensor J (SSJ) precipitating electron and ion spectrometers on board the DMSP satellite is inaccessible during this period. The FY-3E meteorological satellite is a dawn–dusk orbit satellite and orbits the Earth at an altitude of 836 km. The PMA is a similar instrument to the special sensor J (SSJ) precipitating electron and ion spectrometers on board DMSP satellite. The measured electron and ion energy range is 30 eV~ 30 keV.[16]

Super Dual Auroral Radar Network (SuperDARN) consists of over 30 high-frequency radars from ten countries, which extend from the mid-latitude to polar regions and conduct continuous observations of the Earth's upper atmosphere. CN-DARN radars are the new members of the SuperDARN, and have been contributing data to SuperDARN database after the final acceptance of the CMP in 2025. The radars operate continuously and monitor the ionospheric dynamics and other related phenomena. It is a powerful network to obtain the dynamic evolution of global-scale maps of ionospheric irregularities drift and ionospheric plasma convection. The detailed method of obtaining global-scale maps of ionospheric irregularities drift from observations of dozens of radars can be found in many literatures.[17,18]

RESULTS

Solar wind conditions and geomagnetic activity

A strong geomagnetic storm occurred on October 10, triggered by a CME erupted from a sunspot active region 3848 on October 8, 2024. Figure 2 shows the interplanetary magnetic field (IMF), solar wind velocity, and solar wind dynamic pressure at the bow shock nose obtained from the NASA OMNI database (https://omniweb.gsfc.nasa.gov/ow.html). The SYM-H index[19] and geomagnetic three-hourly Kp index[20] are also shown in the figure to indicate the development of the geomagnetic storm. SYM-H index measures the intensity of the storm time ring current, with time resolution of 1 min. The three-hourly planetary Kp index is an index used to monitor geomagnetic activty on a global scale. The shock arrived at the bow shock nose at ~1510 UT, creating a sudden commencement as shown by the SYM-H index. Subsequently, the ring current developed rapidly due to the strong southward component of the IMF (Bz), with the maximum value of the southward IMF component exceeding -40 nT. The SYM-H index dropped to approximately -400 nT at 2315 UT on 10 October, 2024. The solar wind velocity remained between 700 ~ 800 km/s while the dynamic pressure reached 45 nPa. During

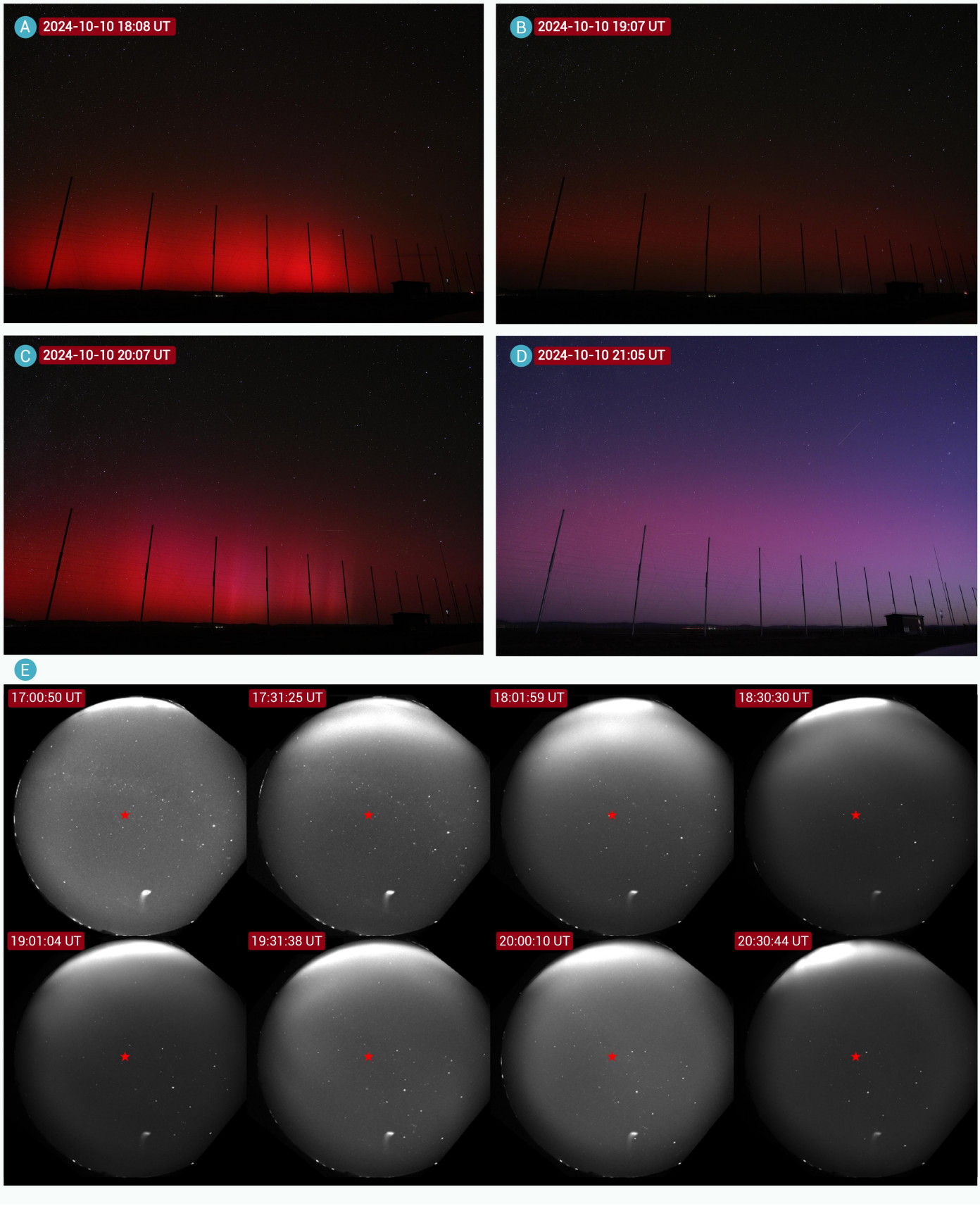

Figure 3. The auroral images captured from the Siziwang Observatory of Space Weather in Inner Mongolia, China Images taken by cameras at (A) 1808 UT, (B) 1907 UT (C) 2007UT, (D) 2105 UT on 10 October 2024. Image data: ISO-4000, 24 mm, f/4, 15s. The background of the photos features the pillars of the main antenna array of the Siziwang West (SZW) radar of the CN-DARN. (E) The auroral activities recorded by the 630 nm airglow all-sky imager at the observatory, where the red star denotes the location of the imager and the top of each image is north.

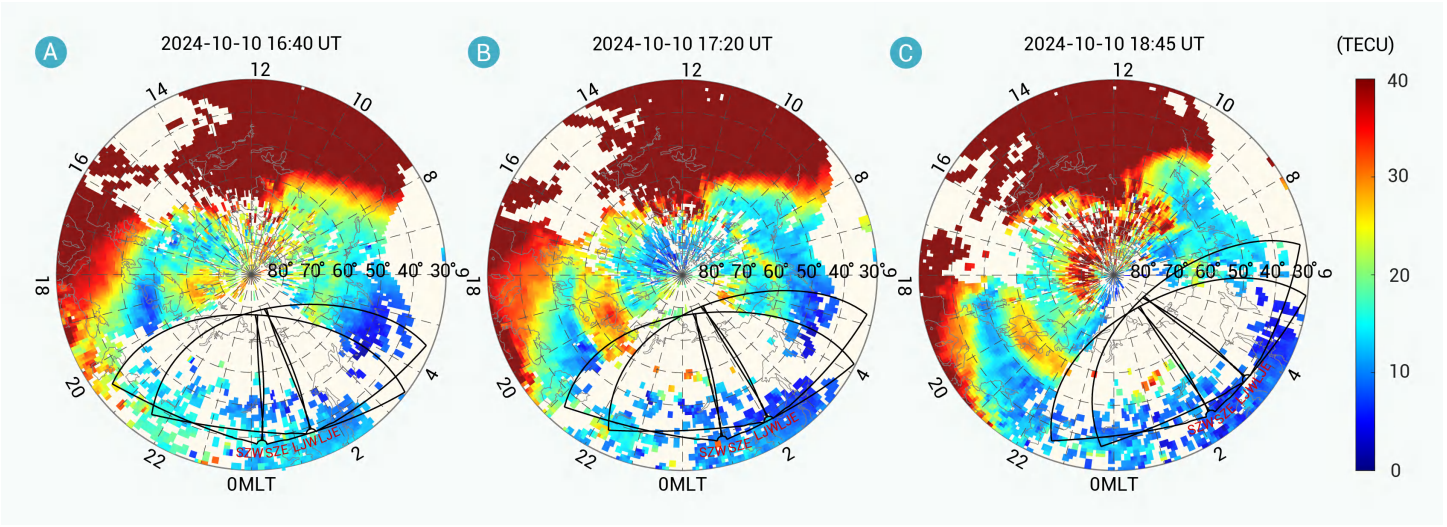

Figure 4. Ionospheric total electron content (TEC) retrieved from global GNSS receivers at (A) 1640 UT, (B) 1720 UT, and (C) 1845 UT The field-of-views of four CN-DARN radars are indicated with solid lines. All maps are presented in the MLAT-MLT coordinate system.

this event, the maximum Kp index approached 9, the highest level of the Kp index scale.

Auroral activity recorded in Inner Mongolia

The geomagnetic storm was so strong that citizens at middle-latitude regions viewed the splendid aurora. The aurora was recorded from Siziwang Observatory of Space Weather in Inner Mongolia (GLAT~41.8° N, MLAT~37.2° N), China for the time interval of 1700 UT~2130 UT on October 10, 2024 (0100 BJT~0530 BJT, Beijing local time on October 11, 2024). For this event, two periods of auroral intensification were observed, characterized by sudden brightness increases and dynamic auroral curtain movements. Figures 3A-D shows the auroral images captured by camera at 1808 UT, 1907 UT, 2007 UT and 2105 UT on October 10 from the location of the main antenna array of the Siziwang West (SZW) radar at Siziwang Observatory of Space Weather. Faint red aurora first appeared on the northwest horizon at 1700 UT, and then the aurora intensified, with the brightening red band attaining its maximum intensity at approximately 1800 UT (Figure 3A). Subsequently, the aurora commenced its weakening phase (Figure 3B). From 2000 UT, the aurora rapidly brightened again, and the bright red band developed with a mixture of structured magenta emission during this period (Figure 3C). After 2030 UT, the aurora gradually dimmed until dawn (Figure 3D). Movie S1 documents the full image sequence, the auroral curtain exhibits rapid eastward movement as the aurora intensifies. Meanwhile, a 630 nm airglow all-sky imager of the CMP deployed at the observatory also recorded the auroral activity. Bright auroral activity appeared at the northern edge of the all-sky imager's FOV (Figure 3E, see Video S2 for the entire image sequence).

Red auroras have been observed occasionally at middle latitudes during strong geomagnetic storms.[21] Broadband electron precipitation with energy range of 30 eV to 30 keV react with oxygen (O) at higher altitudes during storm time substorms can be a possible source that give rise to red auroras visible from the middle latitudes.[22] Because the aurora extended to so high altitude that the top red part can be seen from the middle latitudes. Magenta auroras are rarely seen in mid-latitude areas, may caused by higher energetic particles colliding with nitrogen (N_2^+) in Earth's atmosphere at lower altitude.[2] The plasma analyzer (PMA) on the FY-3E meteorological satellite recorded the energy spectra and energy fluxes of precipitating electrons and ions (30 eV~30 keV) at dawn sector during the two auroral intensification periods are shown in Figure S1. PMA measurements reveal a significant increase in the energy flux of precipitating electrons and ions with energies exceeding 10 keV during the second auroral intensification, indicating the link between the occurrence of magenta auroras and the precipitation of higher-energy particles. High solar activity and the preheating of the atmosphere can promote the occurrence of magenta aurora.[2]

The enhanced auroral particle precipitation strongly increases the total electron content (TEC) within the auroral oval.[23] Figure 4 presents the ionospheric TEC retrieved from global navigation satellite system (GNSS) receivers over the Northern Hemisphere at 1640 UT, 1720 UT, and 1845 UT. Prior to the geomagnetic storm (1640 UT), the nighttime TEC enhancement region resided above 60° MLAT, with a mid-latitude trough with lower TEC existed between 50° and 60° MLAT. As auroral activity intensified from 1700 UT, TEC within the nightside auroral oval increased greatly and expanded equatorward below 60° MLAT as was shown in Figure 4B. Although observation points in the Asian sector are sparse, it is still evident that the maximum TEC within the FOV of the Siziwang (SZW) radar increased greatly, surging from the pre-storm level of 15 TECu to 37.5 TECu at 1845 UT (Figure 4C) during the period of first auroral intensification.

Observations from CN-DARN

Simultaneously with the optical auroral observations, numerous ionospheric irregularities emerged within the FOVs of the CN-DARN radars and rapidly drifted with the auroral activity. Figure 5 shows range-time-intensity (RTI) plots of the LOS Doppler velocities observed by beam 3 of the Siziwang East (SZE) radar, beam 18 of the Siziwang West (SZW) radar, beam 3 of the Longjing East (LJE) radar, and beam 18 of the Longjing West (LJW) radar from 1200 UT to 2400 UT on October 10, 2024; the SYM-H index presented in the last panel to show the development of the geomagnetic storm. The LOS Doppler velocity is scaled according to the color bar shown on the right, with ground backscatter plotted in gray. Negative velocities represent ionospheric irregularities moving away from the radar, while positive velocities indicate ionospheric irregularities moving toward the radar.

Rapid eastward plasma drift. From 1400 UT to 1600 UT, the radars observed some ionospheric irregularities above 65° MLAT, due to the auroral oval being located in the high latitude region before the geomagnetic storm. As the geomagnetic storm developed, the band of ionospheric irregularities observed by the radars rapidly expanded to low latitudes. The ionospheric irregularities were observed between 45°~57° MLAT, lasting approximately 6 hours. The LOS velocity undergoes significant variations with time for each radar beam. Take the observation from beam 15 of LJW radar (Figure 5D), as an example, during the observation period from 1700 UT to 1830 UT, there was a region of high LOS velocity (higher than 600 m/s) between 52° and 57° MLAT. Subsequently, the region of observed irregularities expanded to lower latitudes until 1900 UT. Beginning at 1900 UT, the LOS velocity of the irregularities decreased and showed a trend of moving towards higher latitudes. With the second auroral intensification observed by camera and all-sky imager at approximately 2000 UT, the region of irregularities moved back towards lower latitudes (47°~55° MLAT) with increasing LOS velocity, peaking at 800 m/s by 2040 UT. The region of observed irregularities then moved rapidly to high latitudes due to the recovery of auroral substorm. Afterward, the band of ionospheric irregularities started to rapidly move back to higher

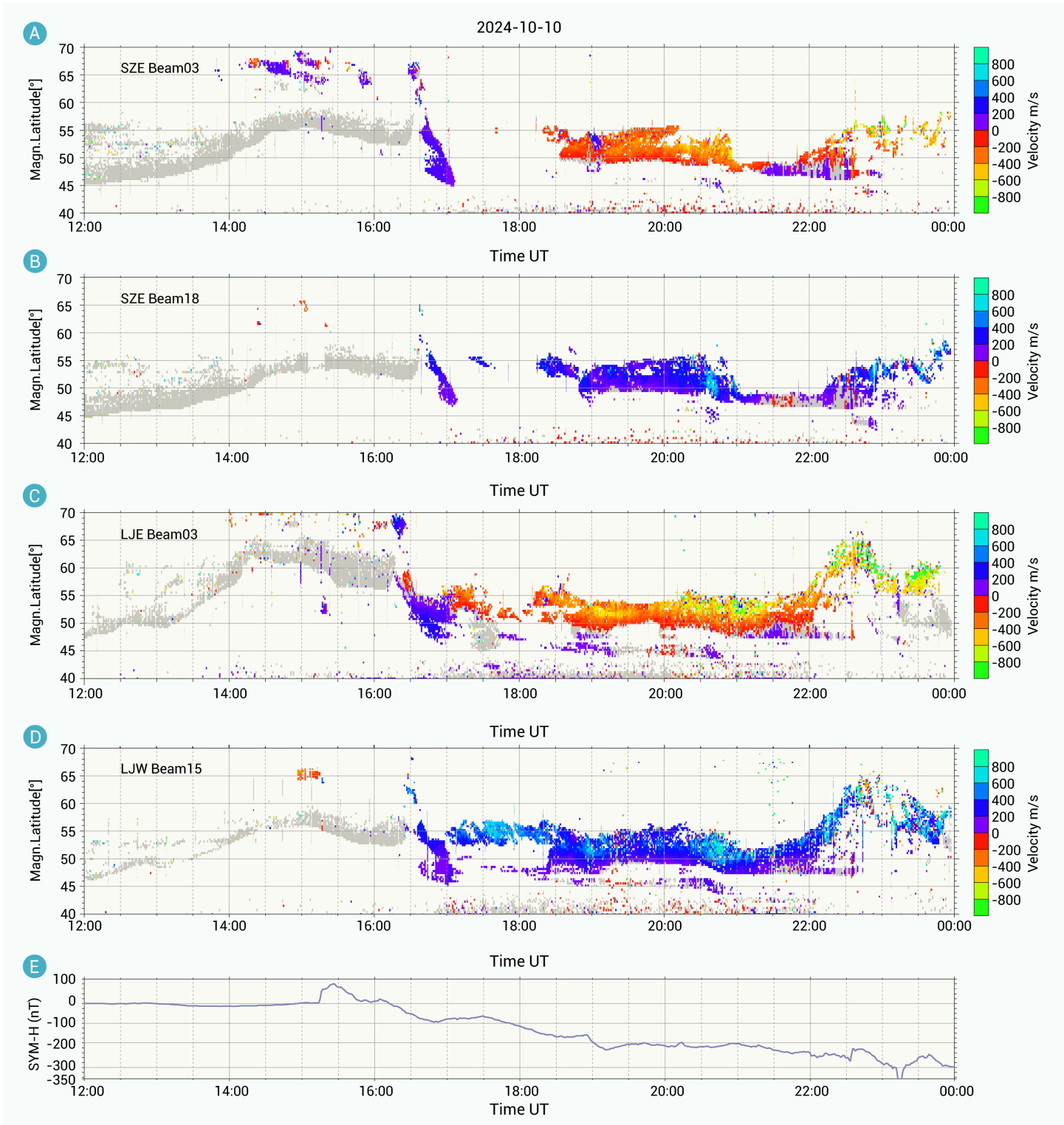

Figure 5. Range-time-intensity (RTI) plots of the ionospheric irregularities LOS velocity observed from CN-DARN radars LOS velocity observed from (A) beam 3 of the Siziwang East (SZE) radar, (B) beam 18 of the Siziwang West (SZW) radar, (C) beam 3 of the Longjing East (LJE) radar, and (D) beam 18 of the Longjing West (LJW) radar. (E) The time series plot of the SYM-H index on October 10, 2024. The LOS velocity is scaled according to the color bar shown on the right, with the ground scatter plotted in gray.

latitudes from 2200 UT. This was related to a northward turning of IMF and the radar gradually rotating with the Earth to the day side. Aurora on the day side of the Earth are generally located at higher latitudes than those on the night side.[1] When the IMF turned strongly southward (Bz~-40 nT) again at ~2230 UT, the band of irregularities moved to lower latitudes again. The LOS velocity of ionospheric irregularities exhibits negative values in observations from the SZE and LJE radars, whereas positive values are recorded by the SZW and LJW radars, collectively indicating an eastward motion of the irregularities.

Dawnside SAPS evolution. To further determine the positional relationship between the observed ionospheric irregularities and the auroral oval, we combine data from CN-DARN radars and space-based LBHS band auroral images from the Defense Meteorological Satellite Program (DMSP) Flight 17 or Flight 18 satellite's SSUSI instrument. Combining ground-based auroral activity observations from the Siziwang Observatory, we found that during the first auroral intensification, the radars observed high-speed eastward drifts of

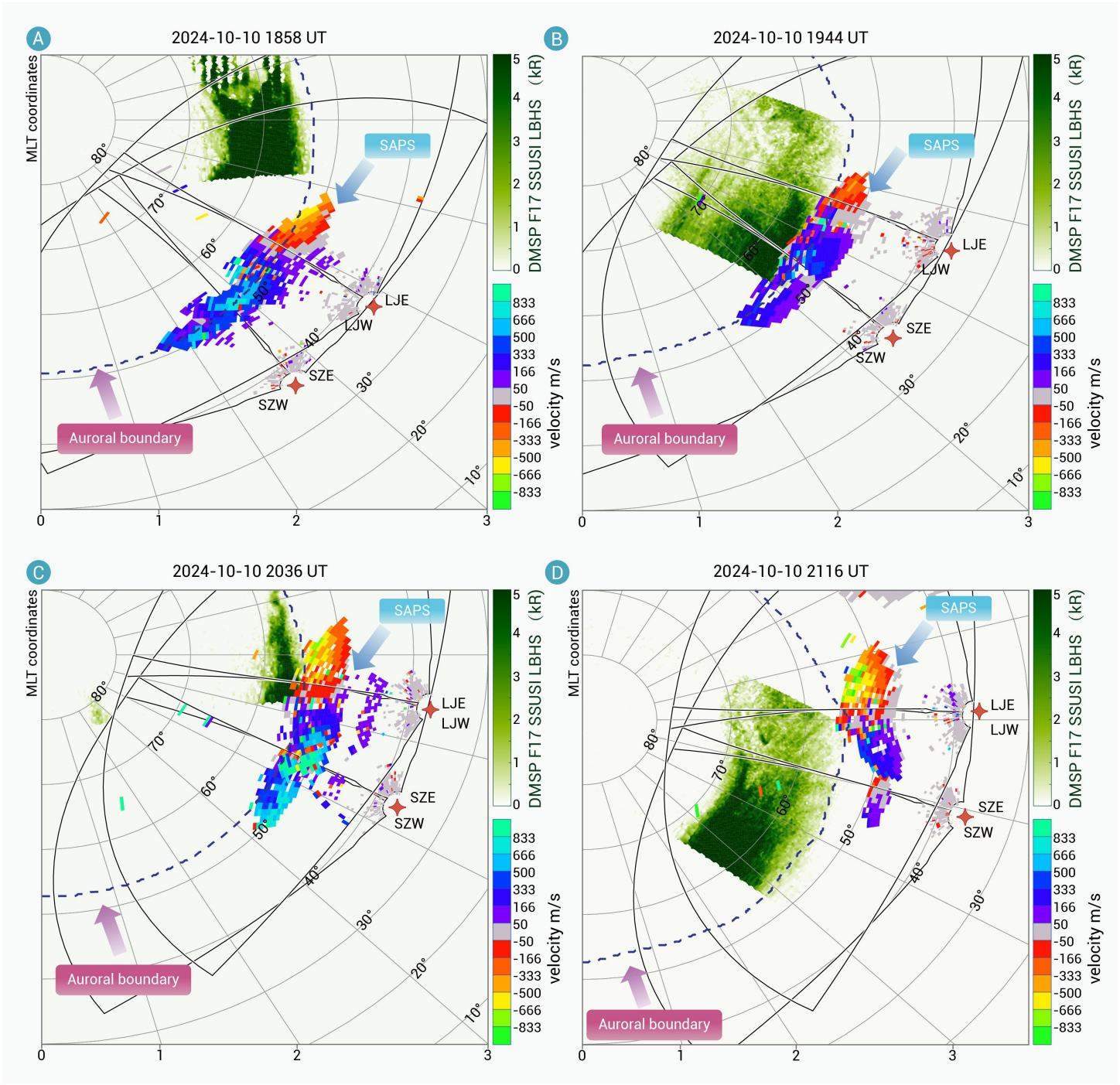

Figure 6. One-minute plots of the LOS velocity of ionospheric irregularities observed by four CN-DARN radars versus magnetic latitude and magnetic local time for (A) 1858 UT, (B) 1944 UT, (C) 2036 UT, and (D) 2116 UT. All maps are presented in the MLAT-MLT coordinate system. The field-of-view of each radar is indicated with solid lines. The radar data has been overlaid onto a swath of the LBHS-band aurora obtained from SSUSI instrument onboard the DMSP F17 or F18 satellite. The dashed line in each map indicates the equatorward boundary of auroral oval.

ionospheric irregularities both within the auroral oval and in the region beyond the equatorward boundary of the auroral oval (referred to as the subauroral region). The observation of high-speed plasma drifts in the subauroral region implies the development of an eastward subauroral polarization stream (SAPS) on the dawnside (Figure 6A). As the aurora weakened, the velocity of the SAPS decreased (Figure 6B). During the second auroral intensification, almost all of the echoes were located in the subauroral region. The velocity of the SAPS increased rapidly, which was faster than that during the first auroral intensification (Figure 6C). This indicates that the auroral intensification is positively correlated with the acceleration of the dawnside SAPS. The observations further suggest that the eastward SAPS on the dawnside can extend from 2 MLT to 7 MLT, demonstrating its extensive longitudinal coverage (Figure 6D).

Subauroral polarization streams (SAPS) were initially defined as a rapid plasma flow occurring on the duskside, characterized by westward convection exceeding 500 m/s. They are located equatorward of auroral precipitation zones and are typically associated with ionospheric troughs.[24] This unique flow phenomenon plays a significant role in the complex dynamics of the Earth's ionosphere and magnetosphere system. The discovery and study of SAPS have deepened our understanding of the energy and mass transfer processes in the high-latitude ionosphere. SAPS are driven by a strong poleward electric field situated equatorward of the electron auroral boundary, which is generated when the boundary of downward Region-2 field-aligned currents (FACs) at duskside shifts equatorward of the electron auroral lati-

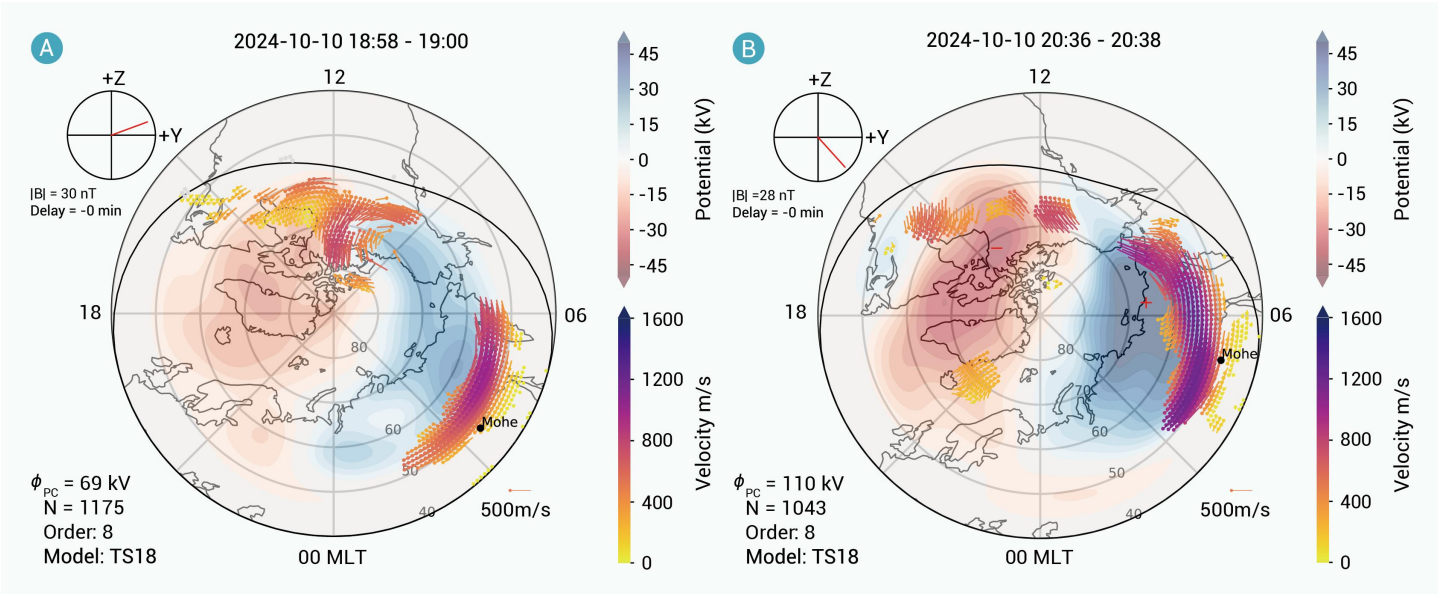

Figure 7. Two snapshots of the Northern Hemisphere ionospheric convection maps on October 10, 2024 Flow vectors indicate the 2-D velocity of ionospheric irregularities and ionospheric plasma, and are only shown in regions where backscatter from ionospheric irregularities was observed. The thick black circle represents the high-latitude convection boundary. The projection of the prevailing IMF (red line) onto the Y-Z GSM plane is shown at the top left of each panel. The cross-polar cap potential (Φpc) determined from the mapping, the number of gridded LOS velocity measurements used in the mapping (N), the order of the spherical harmonic functions of the electrostatic potential (order), and the statistical convection model (TS18)[30] are shown at the bottom left of each panel. Color bars of the flow velocity and equipotential are shown on the right. The large black dot denotes the location of Mohe.

tude.[25] During geomagnetic activity, ions penetrate deeper into the inner magnetosphere than electrons due to their larger mass and longer charge-exchange lifetime, resulting in the ion ring current inner boundary lying closer to Earth than the electron plasma sheet.[26] This radial separation of ion and electron populations creates an outward-directed electric field in the inner magnetosphere, which maps along magnetic field lines to the ionosphere as a poleward electric field. The poleward ionospheric electric field, in turn, drives westward SAPS flow.

In the recent couple of years, a dawnside eastward SAPS has been sporadically identified in DMSP satellite observations during strong geomagnetic storms.[27] However, due to the inherent limitations of satellites pass-by measurements, the dynamic spatiotemporal evolution of this new type of SAPS remains unobserved. Leveraging the continuous and wide-range detection advantages of the ground-based CN-DARN radar network, this study presents the observation of the spatiotemporal evolution of the dawnside eastward SAPS, and uncover the relationship between auroral intensification and the acceleration of dawnside SAPS for the first time. Simulations have shown that during major geomagnetic storms, energetic ions can be transported to the dawnside of the inner magnetosphere by strong magnetospheric convection. This process shifts the boundary of upward Region-2 FACs at dawnside equatorward of the auroral boundary, generating an equatorward electric field that drives eastward dawnside SAPS.[28] The Region-2 FACs are mainly driven by the azimuthal gradient of ring current pressure.[29] The dawnside SAPS observed here occurred during the main phase of the geomagnetic storm, when the ring current was continuously intensifying. As presented in Figure 2, the sustained drop in the SYM-H index between 1600 UT and 2315 UT provides clear indication of the ring current's continuous growth during this period. As further shown in Figure 5, the SZE and LJE radars also detected a weaker westward flow in the lower-latitude region relative to the eastward dawnside SAPS flow, with velocities of less than 200 m/s (indicated by the purple color blocks). In the dawnside, the Region-2 FACs flow into the inner magnetosphere, so the westward flow may exist in the lower latitudes of the footprint of the region-2 FAC during the storm. The observation of the westward flow at lower latitude of the eastward SAPS flow at dawnside further implies the extent of Region-2 FACs, as well as their role in the generation of dawnside SAPS. The positive correlation between energy flux of auroral particle precipitation (Figure S1) and dawnside SAPS velocity revealed in this study implies that variations in the auroral enengy flux may modulate the magnitude of the equatorward polarization electric field that drives the dawnside SAPS, thereby controlling velocity of the dawnside SAPS.

Plasma drift over Northern Hemisphere

A single radar can only measure the LOS velocity of ionospheric irregularities. To derive the two-dimensional motion velocity of these irregularities or ionospheric plasma, data from multiple radars must be intergated.[17] In this study, data from 24 operational SuperDARN radars in the Northern Hemisphere during this day were utilized to construct the northern plasma convection map. Two snapshots of the ionospheric convection maps during this event are shown in Figure 7. In these maps, flow vectors indicate the two-dimensional velocity of ionospheric irregularities. The maximum flow velocities over the Asian region reaches approximately 1000 m/s in Figure 7A and increased to 1200 m/s in Figure 7B. Notably, the area in the Asian sector with velocities exceeding 1000 m/s is substantially larger in Figure 7B compared to Figure 7A. The location of Mohe, the northernmost city in China with geographic coordinates of 53.55° N, 124.33° E and AACGM coordinates of 48.60° N, -161.06° E, is marked by a large black dot. The figures clearly demonstrate that the region of ionospheric irregularities with velocities of 1000 m/s has expanded to Mohe.

During this interval, the equatorward boundary of the auroral oval remained north of 50° MLAT as shown in Figure 6, while Mohe (48.6° MLAT) resided within the sub-auroral region. This indicates that the ionospheric irregularities observed over Mohe were associated with dawnside SAPS, rather than direct particle precipitation within the auroral oval. The study reveals that even when the auroral oval does not expand into Chinese territory, high-speed ionospheric irregularities within dawnside SAPS can manifest over northern China.

High frequency communication loss

High-frequency (HF) communication refers to a technical system that uses electromagnetic waves in the 3–30 MHz frequency band (corresponding to the short-wave band) to achieve long-distance wireless communication. Relying on the refraction and reflection properties of the ionosphere to HF electromagnetic waves, HF communication plays an irreplaceable role in maritime, aviation, emergency communication, and other fields. The operating frequency (8–20 MHz) of CN-DARN radars falls within the short-wave band. By analyzing the backscatters of CN-DARN radars, the impact of the space weather on HF communications can be investigated.

There are two periods: from 1700 UT to 1800 UT and from 2100 UT to 2200 UT, during which the Siziwang East (SZE) and Siziwang West (SZW) radars received very few echoes as Figure 5 shows. This occurred within the two periods of auroral intensifications, which indicates the happening of

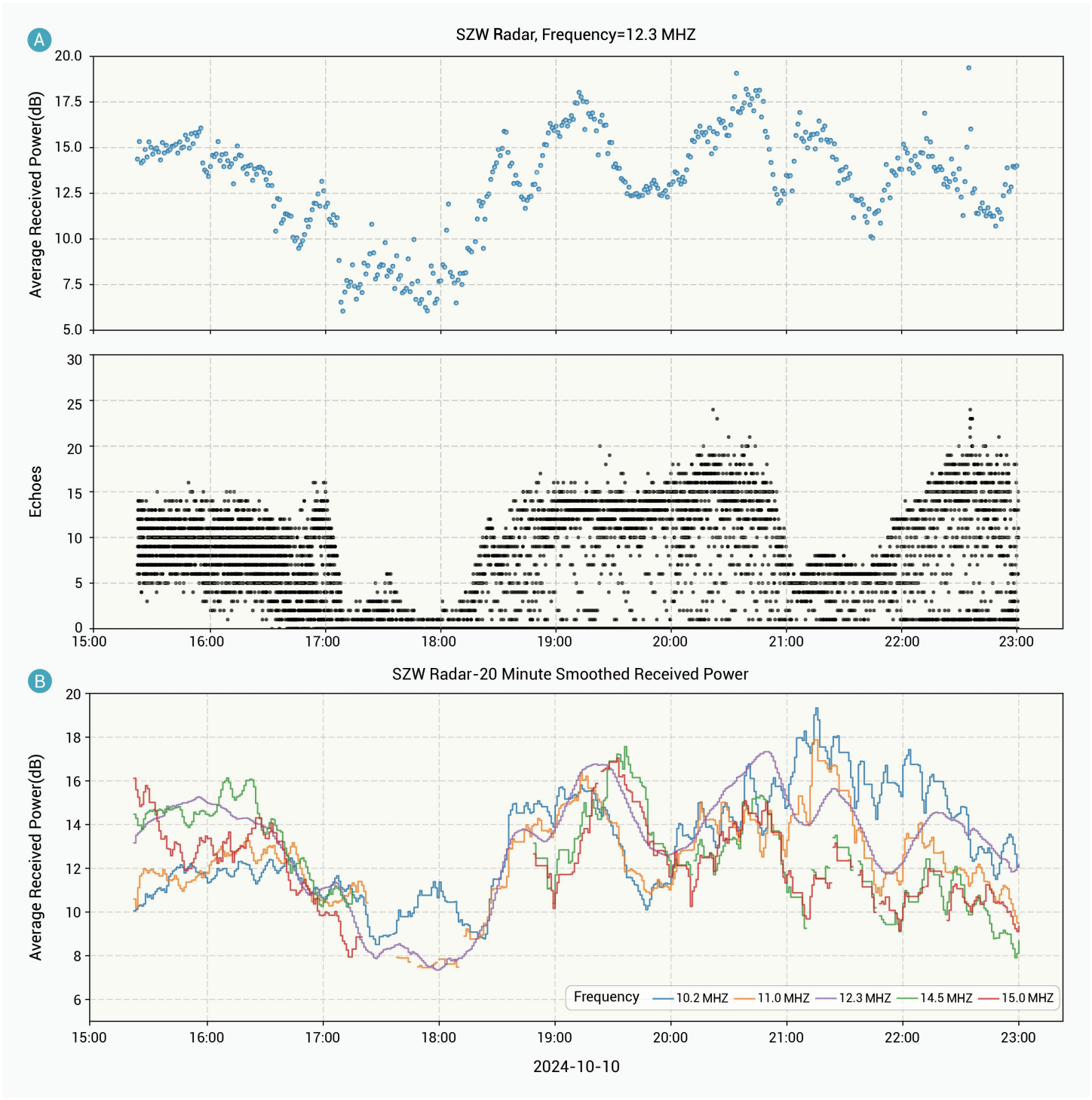

Figure 8. Auroral radio absorption detected by Siziwang West radar on October 10, 2024 (A) Average received power and number of radar echoes in regular 12.3 MHz frequency band. (B) Average received power in multiple frequencies within 10-15 MHz band.

severe auroral radio absorption.[31] This could be attributed to enhanced precipitation in the auroral oval causing an increase in the total electron content (TEC) in the lower layers of the ionosphere.[23] Figure 4 has clearly shown the TEC enhancements during the auroral intensification. According to Figure 8A, during the first auroral intensification, the SZW radar's average received power in the 12.3 MHz frequency band decreased significantly from 16 dB (pre-geomagnetic storm) to 6 dB, a 70% decrease in signal power. And the state of low received power lasted for more than one hour from 1700 UT to 1830 UT. During the second auroral intensification, significant signal degradation was also observed. It is worthwhile to note that all radars were operating in the Normal Sound mode on that day. In this mode, besides conducting the regular observation tasks at fixed frequency point, the radars also scanned through multiple preset frequencies. The results show that all frequencies within the 10-15 MHz band were severely affected by the auroral intensifications (Figure 8B). The observations clearly demonstrate that auroral particle precipitation led to severe HF communication loss over middle and high latitudes of Asia.

DISCUSSION

The geomagnetic storm of May 10–11, 2024, stands as the strongest on record in the 25th Solar Cycle to date, with its SYM-H index reaching to an extreme value of -518 nT. In comparison, the October 10, 2024 geomagnetic storm is slightly less intense with an SYM-H approximately of -400 nT—yet both qualify as severe geomagnetic storms (G5 level). Notably, during both

events, auroral activity was observed across mid-latitude regions of Asia.[2] Amateur photographers across China and Japan captured and shared aurora images and videos online during the events. It is important to clarify, however, that such publicly available visual materials typically lack the contextual observational metadata (e.g. critical timestamps, precise geolocation) required for rigorous scientific analysis. For the October 10, 2024 event, our research team made dedicated camera recordings of auroral activity during this geomagnetic storm at the Siziwang Observatory of Space Weather (Inner Mongolia, China), and integrated these images with data from other instrumental systems at the observatory and on-board satellites to investigate the auroral outbreak process, new physical phenomena linked to the aurora activity and its impacts on the space environment over Asia. This explains our focus on the October 2024 event.

Intense red aurora was observed collocated with the large TEC enhancement over the continental US during the May 2024 storm,[23] which indicated the extremely intense low-energy precipitation during the rapid substorm breakup caused the strong TEC enhancement. The aurora, TEC and energy spectra and fluxes of precipitation observations over Asia during October 2024 storm in this study are consistent with the aforementioned result. By leveraging the technical characteristics of the CN-DARN radars, we conducted a more in-depth analysis of the practical impacts of TEC enhancement (triggered by auroral particle precipitation) on human life, specifically focusing on the attenuation of high-frequency communications.

As the ring current gradually intensified, the CN-DARN radar began detecting rapid ionospheric irregularities drift beyond the equatorward boundary of the auroral oval on the dawnside—indicating the development of the dawnside SAPS. There are several plausible generation mechanisms for ionospheric irregularities within duskside SAPS, such as the gradient-drift instability (GDI), temperature gradient instability and current convective instability.[32] Whether the mechanism responsible for generating ionospheric irregularities within dawnside SAPS aligns with that in duskside SAPS, or what distinct characteristics (if any) set them apart, remains undetermined. To address this problem, additional experimental work and theoretical advancements are necessary.

CONCLUSIONS

In recent years, due to the rapid drift of the Earth's north magnetic pole towards Siberia and the superimposed influence brought about by the ascending phase of the 25th Solar Cycle, auroral activity has been observable in some regions where they were seldom witnessed previously. This not only offers us a visual extravaganza but also prompts us to contemplate the influence of the movement of auroral activities towards lower latitudes on the ionospheric environment. During the severe geomagnetic storm on October 10, 2024, spectacular auroral activity was recorded at the Siziwang Observatory of Space Weather (MLAT~37.2°) in Inner Mongolia, China. In this study, we integrated the recorded auroral images with observations from the CN-DARN radars of CMP and instruments onboard satellites to conduct a detailed analysis of the new physical phenomena associated with this middle-latitude auroral activity, as well as the impacts of the auroral activities on the Asian space environment. The main conclusions are as follows:

1. The CN-DARN radar captured the spatiotemporal dynamic evolution of the dawnside SAPS and, for the first time, identified a positive correlation between the intensity of auroral precipitation energy flux and the velocity of the dawnside SAPS.

2. This study reports that rapidly drifting ionospheric irregularities associated with the middle-latitude auroral activities have extended into Chinese airspace. It further clarifies that those irregularities that have drifted into China are within dawnside SAPS.

3. Through quantitative analysis, this study further establishes that auroral activity induces substantial attenuation of HF communication signals across the Asian region: the signal intensity experiences a maximum attenuation of 70%, and the degradation lasting for over several hours.

In summary, this study marks the first comprehensive analysis of auroral activity captured from unusual latitudes of China and its impact on the ionospheric environment of Asian middle and high latitudes. Our findings on the spatiotemporal evolution characteristics of the dawnside SAPS and its relationship with auroral activity bridge a crucial gap in subauroral research and offer novel insights into complex magnetosphere-ionosphere coupling processes. With continuing increase in geomagnetic latitude, the ionospheric environment in the mid-latitudes of Asia becomes more and more susceptible to the influence of solar disturbances. This work showcases the critical capabilities of the CMP in monitoring the ionospheric environment in the mid- and high-latitudes of Asia. The CMP will play a pivotal role in revealing the mechanisms of the solar wind-magnetosphere-ionosphere coupling system and in space weather warning and forecasting, providing essential support for addressing space environmental challenges.

REFERENCES

1. Akasofu S.I. (1966). The auroral oval, the auroral substorm, and their relations with the internal structure of the magnetosphere. *Planet. Space Sci.* **14**:587–595. DOI:10.1016/0032-0633(66)90043-2
2. Kataoka R., Reddy S.A., Nakano S., et al. (2024). Extended magenta aurora as revealed by citizen science. *Sci. Rep.* **14**:25849. DOI:10.1038/s41598-024-75184-9
3. Livermore P.W., Finlay C.C. and Bayliff M (2020). Recent north magnetic pole acceleration towards Siberia caused by flux lobe elongation. *Nat. Geosci.* **13**:387-391. DOI: 10.1038/s41561-020-0570-9
4. Ross, J.C. (1834). On the position of the North Magnetic Pole. *Phil. Trans. R. Soc.* **124**:47–52. DOI:10.1098/rspl.1830.0139
5. Barraclough D.R., and Malin S.R.C. (1981). 150 years of the North Magnetic Pole. *Nature* **291**:377–377. DOI:10.1038/291377a0
6. Chulliat A., Brown W., Alken P., et al. (2020). The US/UK world magnetic model for 2020-2025 : *Tech. Rep.* DOI: 10.25923/ytk1-yx35
7. Tsyganenko N.A. (2019). Secular drift of the Auroral ovals: How fast do they actually move. *Geophys. Res. Lett.* **46**:3017–3023. DOI:10.1029/2019GL082159
8. Zhang J., Lan A., Yan J., et al. (2024). Development of the Chinese Dual Auroral Radar Network and preliminary results. *Space Weather* **22**:e2024SW004131. DOI:10.1029/2024SW004131
9. Wang C., Xu J., Chen Z., et al. (2024). China's ground-based space environment monitoring network—Chinese Meridian Project (CMP). *Space Weather* **22**:e2024SW003972. DOI:10.1029/2024SW003972
10. Chisham G., Lester M., Milan S.E., et al. (2007). A decade of the Super Dual Auroral Radar Network (SuperDARN): scientific achievements, new techniques and future directions. *Surv. Geophys.* **28**:33–109. DOI:10.1007/s10712-007-9017-8
11. Nishitani N., Ruohoniemi J.M., Lester M., et al. (2019). Review of the accomplishments of mid-latitude Super Dual Auroral Radar Network (SuperDARN) HF radars. *Prog. Earth Planet. Sci.* **6**:27. DOI:10.1186/s40645-019-0270-5
12. Greenwald R.A., Baker K.B., Hutchins R.A., et al. (1985). An HF phased-array radar for studying small-scale structure in the high-latitude ionosphere. *Radio Science* **20**:63–79. DOI:10.1029/RS020i001p00063
13. Shepherd S.G. (2014). Altitude - adjusted corrected geomagnetic coordinates: Definition and functional approximations. *J. Geophys. Res.* **119**:7501–7521. DOI:10.1002/2014JA020264
14. Jonkers A.R.T., Jackson A., and Murray A. (2003). Four centuries of geomagnetic data from historical records. *Rev. Geophys.* **41**. DOI: 10.1029/2002RG000115
15. Sotirelis T., Korth H., Hsieh S.-Y., et al. (2013). Empirical relationship between electron precipitation and far-ultraviolet auroral emissions from DMSP observations. *J. Geophys. Res.* **118**:1203–1209. DOI:10.1002/jgra.50157
16. Wang X., Zhang X., Wang J., et al. (2023). Plasma analyzer for the Chinese FY-3E satellite: In-orbit performance and ground calibration. *Atmosphere* **14**:1665. DOI:10.3390/atmos14111665
17. Ruohoniemi J., and Baker K. (1998). Large - scale imaging of high - latitude convection with Super Dual Auroral Radar Network HF radar observations. *J. Geophys. Res.* **103**:20797–20811. DOI:10.1029/98JA01288
18. Zhang J.J., Wang W., Wang C., et al. (2020). First observation of ionospheric convection from the Jiamusi HF radar during a strong geomagnetic storm. *Earth Space Sci.* **7**:e2019EA000911. DOI:10.1029/2019ea000911
19. Wanliss J.A., and Showalter K.M. (2006). High-resolution global storm index: Dst versus SYM-H. *J. Geophys. Res.* **111**:A02202. DOI: 10.1029/2005ja011034
20. Matzka J., Stolle C., Yamazaki Y., et al. (2021). The geomagnetic Kp index and derived indices of geomagnetic activity. *Space Weather* **19**:e2020SW002641. DOI:10.1029/2020SW002641
21. Kataoka R., Miyoshi Y., Shiokawa K., et al. (2024). Magnetic storm-time red aurora as seen from Hokkaido, Japan on 1 December 2023 associated with high-density solar wind. *Geophys. Res. Lett.* **51**:e2024GL108778. DOI:10.1029/2024GL108778
22. Shiokaw K., Meng C.-I., Reeves G.D., et al. (1997). A multievent study of broadband electrons observed by the DMSP satellites and their relation to red aurora observed at midlatitude stations. *J. Geophys. Res.* **102**:14237–14253. DOI:10.1029/97JA00741
23. Foster J.C., Erickson P.J., Nishimura Y., et al. (2024). Imaging the May 2024 extreme aurora with ionospheric total electron content. *Geophys. Res. Lett.* **51**:e2024GL111981. DOI:10.1029/2024GL111981
24. Foster J.C., and Vo H.B. (2002). Average characteristics and activity dependence of the subauroral polarization stream. *J. Geophys. Res.* **107**:1475. DOI: 10.1029/2002ja009409

25. Anderson P.C., Hanson W.B., Heelis R.A., et al. (1993). A proposed production model of rapid subauroral ion drifts and their relationship to substorm evolution. *J. Geophys. Res.* **98**:6069–6078. DOI:10.1029/92JA01975
26. Califf S., Li X., Wolf R.A., et al. (2016). Large-amplitude electric fields in the inner magnetosphere: Van Allen Probes observations of subauroral polarization streams. *J. Geophys. Res.* **121**:5294–5306. DOI:10.1002/2015JA022252
27. Horvath I., and Lovell B.C. (2022). Newly formed dawnside, duskside, and nightside subauroral flows developed during magnetically active times. *J. Geophys. Res.* **127**:e2021JA030215. DOI:10.1029/2021JA030215
28. Lin D., Wang W., Merkin V.G., et al. (2022). Origin of dawnside subauroral polarization streams during major geomagnetic storms. *AGU Adv.* **3**:e2022AV000708. DOI:10.1029/2022AV000708
29. Vasyliunas V.M. (1970). Mathematical models of magnetospheric convection and its coupling to the ionosphere. In B.M. McCormac (ed). Particles and Fields in the Magnetosphere. Dordrecht. DOI:10.1007/978-94-010-3284-1_6
30. Thomas E.G., and Shepherd S.G. (2018). Statistical patterns of ionospheric convection derived from mid-latitude, high-latitude, and polar SuperDARN HF radar observations. *J. Geophys. Res.* **123**:3196–3216. DOI:10.1002/2018JA025280
31. Nielsen E., and Axford W.I. (1977). Small scale auroral absorption events associated with substorms. *Nature* **267**:502–504. DOI:10.1038/267502a0
32. Mishin E., and Streltsov A. (2021). Mesoscale and small-scale structure of the subauroral geospace. In Ionosphere Dynamics and Applications, pp:139-158. DOI: 10.1002/9781119815617.ch8

FUNDING AND ACKNOWLEDGMENTS

This work was supported by the National Key R&D Program of China 2022YFF0504400. The work was also supported by NNSFC Grants 42188101 and 42174210 and the Climbing Program of NSSC (E1PD3001). SGS and EGT acknowledge support from the National Science Foundation under grant AGS-1934997. The constructions of the CN - DARN, all-sky imager, magnetometers derived the Chinese SYM-H index were made possible by funds provided by the Chinese Meridian Project Phase II. The authors acknowledge the use of SSUSI data from DMSP satellites, and PMA data from FY-3E satellite. We also acknowledge CDAWeb of the Goddard Space Flight Center for use of the solar wind data and SYM - H index from the OMNI database. We thank the GFZ German Research Centre for Geosciences for providing the Kp index. The authors acknowledge the use of SuperDARN data. SuperDARN is a network of radars funded by the national scientific funding agencies of Australia, Canada, China, France, Italy, Japan, Norway, South Africa, the United Kingdom, and the United States of America. The funders had no role in study design, data collection and analysis, decision to publish, or preparation of the manuscript.

AUTHOR CONTRIBUTIONS

Jiaojiao Zhang, Chi Wang and Hui Li conceived this study. Jiaojiao Zhang, Xiang Deng, Hang Li, Wei Wang, Ailan Lan prepared and processed the CN-DARN data, Xiang Deng prepared the auroral data recorded by camera, Jiyao Xu and Jianyun Liang prepared the auroral images recoded by all-sky imagers, Hui Li and Ziqian Liu prepared the Chinese SYM-H index data, Simon G. Shepherd and Evan G. Thomas provided the AACGM algorithm. Wei Wang, Fuqing Huang, and Zheng Wang prepared and processed the TEC data. Xinyue Wang, Xianguo Zhang and Weiguo Zong prepared and processed the PMA data. Jiaojiao Zhang prepared the figures and wrote the initial draft, all authors review the manuscript. All authors contributed to the manuscript and approved the final version.

DECLARATION OF INTERESTS

The authors declare no competing interests.

DATA AND CODE AVAILABILITY

The data of CN-DARN radars used in this study is available at Science Data Bank: https://doi.org/10.57760/sciencedb.space.02321. The SSUSI auroral data are available at this site (http://ssusi.jhuapl.edu/). Solar wind data and SYM-H index can be obtained from OMNI database on the CDAweb (https://omniweb.gsfc.nasa.gov/ow.html). Kp index is downloaded from: https://kp.gfz-potsdam.de/en/. The TEC data products can access through the Madrigal distribution data system (http://www.openmadrigal.org). The data of PMA on board Fengyun-3E is provided by National Satellite Meteorological Center, China Meteorological Administration (https://data.nsmc.org.cn/DataPortal/cn/home/index.html).

SUPPLEMENTAL INFORMATION

It can be found online at https://doi.org/10.59717/j.xinn-geo.2026.100197

The Innovation Geoscience, *Volume 4*

Supplemental Information

Auroral activity observed from unusual latitudes in Chinaand its underlying significance

DOI: https://doi.org/10.59717/j.xinn-geo.2026.100197

Jiaojiao Zhang, Xiang Deng, Jiyao Xu, Hui Li, Hang Li, Wei Wang, Jianyun Liang, Simon G. Shepherd, Evan G. Thomas, Ailan Lan, Jingye Yan, Zheng Wang, Qing-He Zhang, Ziqian Liu, Xinyue Wang, Fuqing Huang, Xianguo Zhang, Weiguo Zong, Chi Wang

Figure S1 Energy-time spectra and energy fluxes of precipitating electrons and ions observed by plasma analyzer (PMA) on-board FY-3E meteorological satellite during (a) the first auroral intensification and (b) the second auroral intensification in the dawn sector.

Movie S1. The auroral activities recorded at Siziwang Observatory of Space Weather by cameras during 10-11 October 2024 geomagnetic storms.

Movie S2. The auroral activities recorded at Siziwang Observatory of Space Weather by 630 nm all-sky imager during 10-11 October 2024 geomagnetic storms.

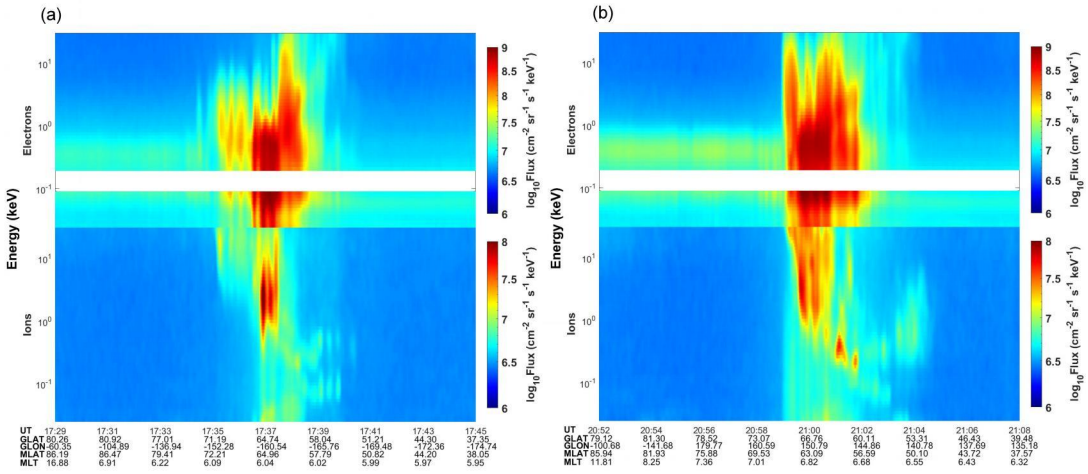

Fig. S1 Energy-time spectra and energy fluxes of precipitating electrons and ions observed by plasma analyzer (PMA) on-board FY-3E meteorological satellite during (a) the first auroral intensification and (b) the second auroral intensification in the dawn sector. Universal time (UT) and satellite locations (geographic latitude, geographic longitude, magnetic latitude and magnetic local time) are shown at the bottom of each panel. The blank in the electron energy spectra is caused by the malfunction of three channels.

Movie S1. The auroral activities recorded at Siziwang Observatory of Space Weather by cameras during 10-11 October 2024 geomagnetic storms.

Movie S2. The auroral activities recorded at Siziwang Observatory of Space Weather by 630 nm all-sky imager during 10-11 October 2024 geomagnetic storms.